THE ASTROPHYSICAL JOURNAL, 532:L117–L120, 2000 April 1

A SPATIALLY RESOLVED PLERIONIC X-RAY NEBULA AROUND PSR B0540−69

E. V. GOTTHELF[1] AND Q. DANIEL WANG[2]

Received 2000 January 10; accepted 2000 February 10; published 2000 March 14

ABSTRACT

We present a high-resolution *Chandra* X-ray observation of PSR B0540−69, the Crab-like 50 ms pulsar in the Large Magellanic Cloud. We use phase-resolved imaging to decompose the extended X-ray emission, as expected of a synchrotron nebula, from the pointlike emission of the pulsar. The image of the pulsed X-ray emission shows a well-defined point-spread function of the observation, while the resolved nebula has a morphology and size remarkably similar to the Crab nebula, including evidence for a jetlike feature from PSR B0540−69. The patchy outer shell, which most likely represents the expanding blast wave of the supernova, is reminiscent of that seen in radio. Based on morphology, size, and energetics, there can be little doubt that SNR B0540−69 is an analogous system to the Crab but located in our neighboring galaxy.

Subject headings: pulsars: general — pulsars: individual (PSR B0540−69) — stars: neutron — supernova remnants — X-rays: general

1. INTRODUCTION

The X-ray–bright 50 ms pulsar PSR B0540−69 was discovered in the N158A nebula of the Large Magellanic Cloud (LMC) and has long been compared to the Crab pulsar (Seward, Harnden, & Helfand 1984). Based on its timing and spectral properties, the two rotation-powered pulsars are very similar with a spin period of 50 versus 33 ms and a spin-down rate of 4.8×10^{-13} versus 4.0×10^{-13} s s^{-1} for PSR B0540−69 and the Crab, respectively. From these quantities, assuming the standard magnetic dipole pulsar model, one can infer a characteristic age (1.7 vs. 1.2 kyr), spin-down energy (2.0×10^{38} vs. 6.5×10^{38} ergs s^{-1}), and surface magnetic field strength (5.0×10^{12} vs. 3.8×10^{12} G) for PSR B0540−69 and the Crab, respectively. This similarity suggests that PSR B0540−69 could be accompanied by a "plerion," a pulsar-driven wind nebula (Weiler & Sramek 1988), reminiscent of that seen for the Crab.

Indeed, there are several lines of evidence indicating the presence of a plerion in the vicinity of PSR B0540−69. Chanan, Helfand, & Reynolds (1984) detected a polarized optical nebula of half-power diameter ∼4″ around the pulsar. This apparent synchrotron nebula was also resolved (although barely) in a radio image presented by Manchester, Staveley-Smith, & Kesteven (1993) and in a *ROSAT* high-resolution imager observation by Seward & Harnden (1994). Furthermore, the overall X-ray spectrum of PSR B0540−69 and its remnant (SNR B0540−69) is well characterized by a power law, as expected if the emission is predominantly nonthermal (Clark et al. 1982; Wang & Gotthelf 1998a).

The *ROSAT* observation also revealed a faint X-ray–emitting shell, ∼15 pc in size surrounding the pulsar. This shell contributes less than 20% to the total luminosity of $\sim 1.0 \times 10^{37}$ ergs s^{-1} in the *ROSAT* 0.1–2 keV band and is likely the supernova remnant (SNR) associated with the pulsar (Seward & Harden 1994). However, no evidence has yet been found for a similar X-ray–emitting shell or a shell-like SNR around the Crab (e.g., see discussion in Jones et al. 1998).

In this Letter, we report new results on SNR B0540−69 based on a recent observation acquired with the *Chandra* High-Resolution Camera. This observation enables us for the first time to distinguish morphological details of the nebula around PSR B0540−69. We analyze phase-dependent images and resolve the expected plerion-like nebula from the pointlike pulsar emission. This allows us to identify features similar to those seen from the Crab nebula; we present morphological evidence for a torus of X-ray emission, which most likely represents shocked pulsar wind materials and a likely X-ray jet emanating from the pulsar. We discuss the implications of the results in the context of the pulsar-nebula system. Throughout the Letter, we adopt a distance of 51 kpc for the LMC.

2. OBSERVATION

The *Chandra* observatory (Weisskopf, O'Dell, & van Speybroeck 1996) observed SNR B0540−69 on 1999 August 31 as part of the initial calibration of the High-Resolution Camera (HRC; Murray et al. 1997). A total of 19.4 ks of data were collected during a portion of the orbit that avoided regions of high background contamination such as from bright Earth and radiation belt passages. The remnant was centered on the on-axis position of the HRC at which the point-spread function (PSF) has a half-power radius (the radius enclosing 50% of total source counts) of ∼0.″5. Time-tagged photons were acquired with 15.6 μs precision, and the arrival times were corrected to the solar system barycenter using a beta version of AXBARY available from the *Chandra* X-Ray Center FTP site (A. Rots 1999, private communication). While the detector is sensitive to X-rays over a 0.1−10.0 keV range, there is essentially no energy information available. We analyzed event data calibrated by the initial processing and dated 1999 September 12, which was made available through the *Chandra* public archive. In addition to the standard processing, the event data were further filtered to reduce the instrumental background and to remove "ghost image" artifacts using a beta version of HRC_SCREEN (S. Murray 2000, private communication). We extracted 1024 × 1024 pixel images centered on the pulsar rebinned by a factor of 2 from the native HRC pixel size of 0.″13175 per side.

[1] Columbia Astrophysics Laboratory, Columbia University, 550 West 120th Street, New York, NY 10027; evg@astro.columbia.edu.

[2] Department of Physics and Astronomy, University of Massachusetts, B-524 Lederle Graduate Research Center, Amherst, MA 01003; wqd@astro.umass.edu.

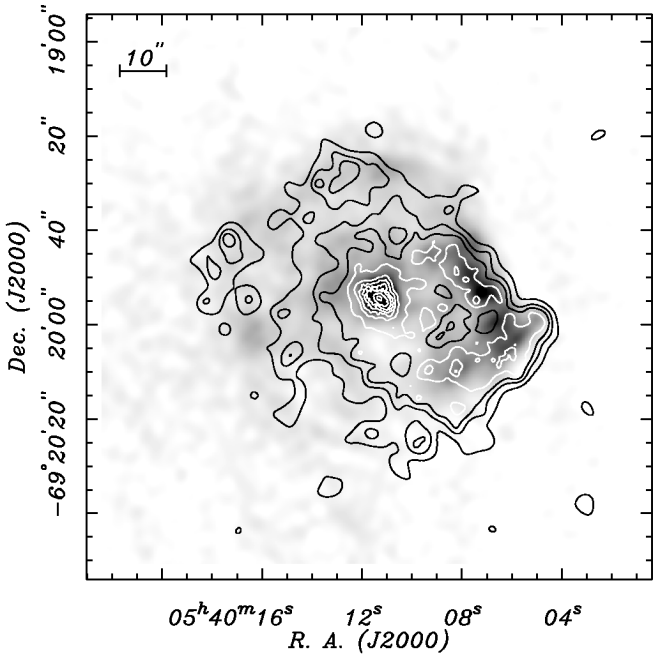

FIG. 1.—Overall X-ray and radio view of the region of SNR 0540-69 containing the central 50 ms pulsar PSR B0540−69. The contours denote the *Chandra* HRC X-ray intensity distribution; the levels are 0.005, 0.01, 0.015, 0.02, 0.04, 0.1, 0.3, 1, 3, 10, and 30 counts s^{-1} $arcsec^{-2}$. The gray-scale map shows the 6 cm radio emission, which traces the approximately circular remnant. The radio map is from Manchester et al. (1993) and has a beam size with half-power width of ∼5.

3. RESULTS

A global view of N158A and its environment as seen by the *Chandra* HRC is shown in Figure 1 (*contours*) and Figure 2 (*gray scale*). The large-scale X-ray enhancement on scales up to ∼1′ is the previously resolved shell-like emission (Seward & Harnden 1994). In fact, the X-ray and radio emission together outlines a nearly circular morphology around PSR B0540−69. Clearly, the shell represents the blast wave of SNR B0540−69. The X-ray intensity distribution within the remnant appears rather patchy. While the southwest X-ray enhancement is a good tracer of the radio and optical emission peaks, there is no general correlation between fainter radio and X-ray features.

The superb spatial resolution of the *Chandra* observation further allows for a close-up of the immediate vicinity of PSR B0540−69 (Fig. 2*b*). The presence of a diffuse plerion-like nebula around the pulsar is apparent. To decompose the nebula emission from the pulsar contribution, we conducted phase-resolved image analysis. This enables us to estimate the local PSF based on the pulsed, pointlike emission from the pulsar and to quantify the extended, unpulsed nebula radiation.

First, we must determine the pulse period at the current epoch. We constructed a periodigram around a narrow range of periods centered on the expected period ±0.1 ms, sampled in increments of $0.05(P^2/T)$, where T is the observation duration and P is the test period. For each trial period, we folded photons extracted from a 1.″0 aperture centered on the bootstrapped pulsar position (see below) into 20 phase bins and computed the χ^2 of the resultant profile. We find a highly significant signal (>56 σ) at P = 50.508132(6) ms at epoch 51,421.630741 MJD; the uncertainty is estimated according to the method of Leahy (1987). We have assumed a period derivative of $\dot{P}$ = 4.789342×10^{-13} for the data epoch (Deeter, Nagase, & Boynton 1999). In Figure 3 we display the resultant light curve

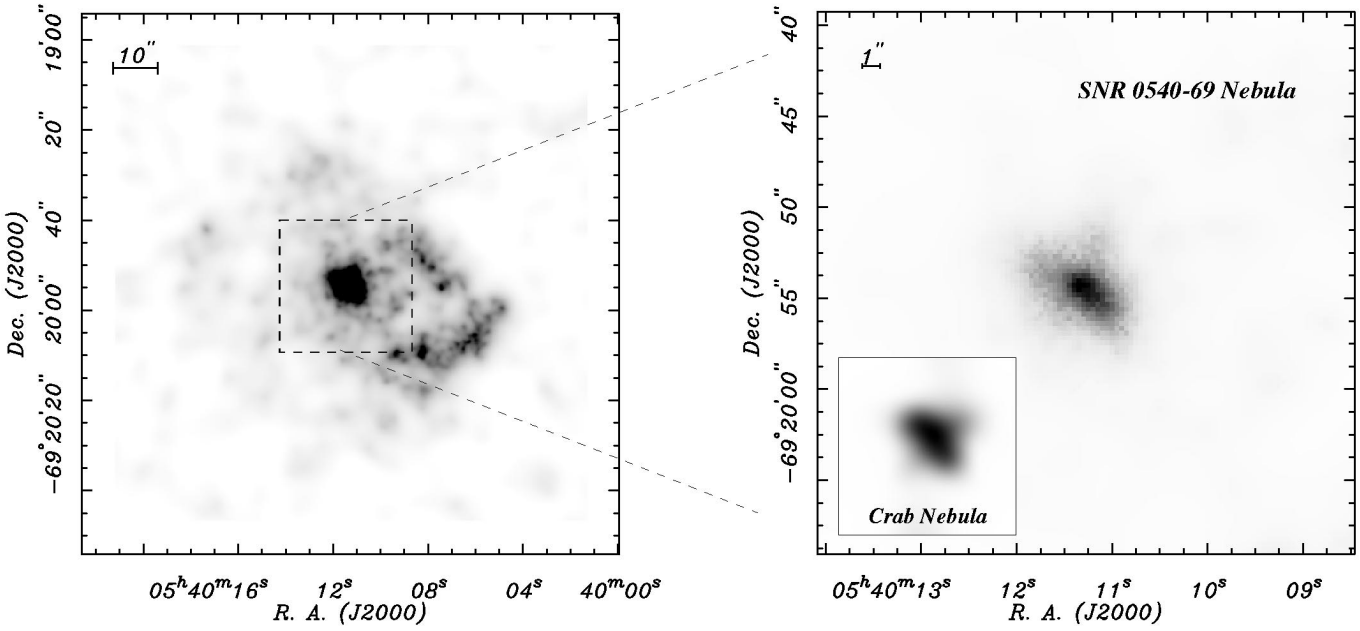

FIG. 2.—X-ray intensity distribution around the region containing the 50 ms pulsar PSR B0540−69. *Left: Chandra* HRC broad energy band image centered on the pulsar. The image has been adaptively smoothed using a minimum signal-to-noise ratio of 6 and the intensity scale chosen to highlight the diffuse SNR emission surrounding the bright pulsar nebula, which is fully saturated in this image. The central box delineates the region enlarged and displayed in the right panel. *Right:* Close-up image around the pulsar, displayed scaled by the square root of intensity. *Inset:* Crab nebula image, placed at the distance of the LMC (assuming a distance to the Crab of 2 kpc) and blurred to the HRC resolution. Notice the similar size, shape, and overall brightness morphology compared to PSR B0540−69.

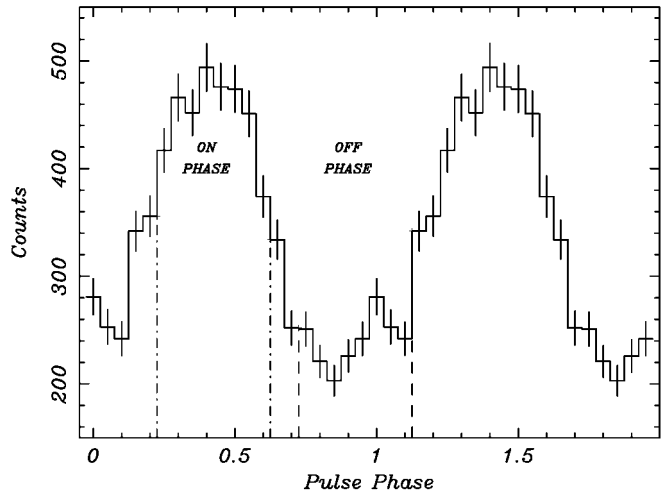

FIG. 3.—HRC light curve (0.4–10 keV) for PSR B0540−69 folded at the ephemeris given in the text. Two periods are shown for clarity. The two sets of vertical bars denote the two phase regions (on/off) used to isolate the nebula from the pulsar emission. The light curve has been extracted from a 1″ radius aperture centered on the pulsar.

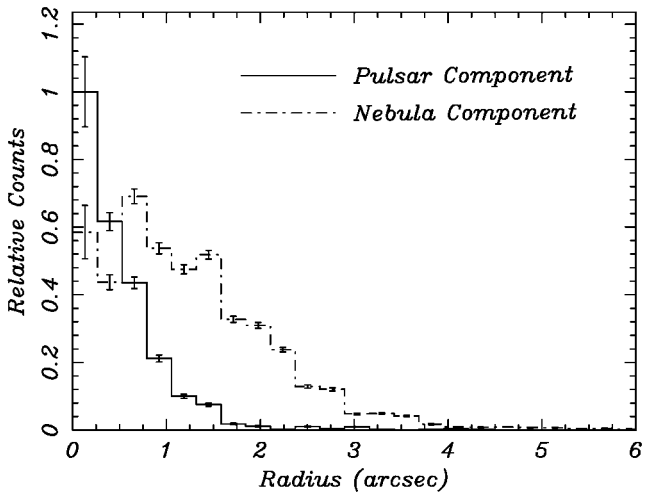

FIG. 5.—HRC radial intensity distributions around the pointlike emission peak of PSR B0540−69. The pulsar radial profile (*solid line*) is consistent with the HRC point-spread function. The nebula profile (*dotted line*) is significantly extended, the enhancement between 0.″1−1.″5 is due to the relatively bright southwest nebula region.

folded at the peak period which, as expected, is roughly sinusoidal and modulated with a ∼40% pulse fraction (defined as the amplitude divided by the mean).

Next, we defined two regions in the phase space, on- and off-pulse, by selecting eight adjacent phase bins corresponding to the peak and trough of the pulse profile. The on-pulse image with the off-pulse image subtracted is presented in Figure 4*b*. This image reproduced the expected PSF with no evidence of asymmetric deviations, as might be caused by poor aspect reconstruction, like that typically found for *ROSAT* images. Figure 5 presents average radial intensity distributions around the centroid of the pointlike source.

By subtracting the normalized pulsar image (Fig. 4*b*), we are able to construct an image of the nebula emission (Fig. 4*c*) alone. The subtracted image is scaled to compensate for both the relative phase coverage and for a 21% unpulsed emission contribution, estimated by minimizing a pointlike contribution at the pulsar position of the nebula image. As shown in Figure 4*c*, the extended emission is distinctly different from the pointlike image of the pulsed emission from the pulsar. The primary feature is the northeast-southwest elongated feature, which is morphologically symmetric relative to the pulsar and extends about ∼2.″5 on both sides of the pulsar. However, the observed emission on the southwest side appears twice as strong compared to the northeast side, with an average intensity of $\sim 7.5 \times 10^{-2}$ counts s^{-1} arcsec^{-2}. Because the central core of the distribution is significantly brighter than the extended features and the subtraction of the pulsar contribution is somewhat arbitrary, the exact intensity distribution is uncertain.

There is also marginal evidence for a jetlike feature emanating from the pulsar. This emission, most apparent in the northwest and extending about 3″, is nearly perpendicular to the northeast-southwest elongated nebula and is slightly bent toward north. The integrated emission of the jetlike feature is roughly $\sim 3.1 \times 10^{-2}$ counts s^{-1}. The configuration of the jet feature relative to the nebula is remarkably similar to that of the Crab nebula as seen by *ROSAT* and which is now clearly resolved with *Chandra* (see *Chandra* publicity photo[3]).

In short, the X-ray emission can be decomposed into three major morphological components: a pointlike source, the sur-

[3] Available at http://xrtpub.harvard.edu/photo/0052/0052_hand.html.

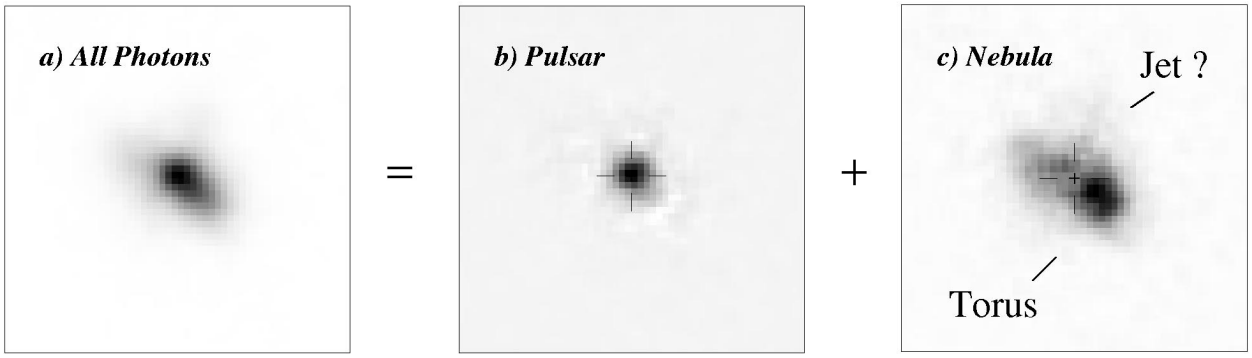

FIG. 4.—Phase-subtracted X-ray intensity maps of PSR B0540−69. (*a*) Before phase-subtraction, image of the pulsar and nebula (all photons), same as the right panel of Fig. 2. (*b*) Pulsar image containing the pulsed photons only. This is in excellent representation of the HRC point-spread function, consistent with the ground calibration. (*c*) Same region after subtracting the pulsar's contribution to the total flux (see text for details); this provides a good estimate of the nebula emission surrounding the pulsar. The cross marks the pulsar's centroid. The three maps are identically sized and linearly scaled in intensity.

rounding nebula which shows evidence for a jet feature, and a patchy SNR shell. Table 1 summarizes the properties of the individual components, including their PSF-corrected sizes and intensities.

TABLE 1

HRC Spatial Components of SNR B0540−69

Component[a]	Count Rate (counts s^{-1})	Size and Shape
Pulsar:[b]		
Pulsed	0.14	Pointlike
Unpulsed	0.18	Pointlike
Nebula	0.8	5″ × 3″ NE-SW
Jet	0.03	3″ long SE-NW
SNR shell	0.2	~1′ diameter

[a] See § 3.

[b] X-ray emission from a 2″ radius aperture around the pulsar.

4. DISCUSSIONS

A comparison between the X-ray–emitting nebula around PSR B0540−69 and the Crab nebula (see *Chandra* publicity photo) is very informative. The Crab nebula image shows a torus of X-ray–emitting loops, which most likely represents shocked pulsar wind materials consisting of magnetic waves and ultrarelativistic particles. Also clear are the two jets of X-ray–emitting material emanating from the Crab pulsar in the direction perpendicular to the major axis of the torus. We speculate that the nebula around PSR B0540−69 has a similar structure. In fact, at the spatial resolution of *Chandra* at the LMC, the size, morphology, and surface intensity of the two nebulae are all remarkably similar (Fig. 2*b*).

Assuming a power-law spectrum for the X-ray emission from the SNR B0540−69 nebula of photon index 2.0 and $N_{\rm H} = 4 \times 10^{21}$ cm^2 (Finley et al. 1993; Wang & Gotthelf 1998a), the conversion between the count rate and the energy flux in the standard 1.0–10 keV band is $\sim 1 \times 10^{-10}$ ergs s^{-1} cm^{-2} (counts s^{-1})$^{-1}$. The corresponding total luminosity of the nebula is $\sim 2.7 \times 10^{37}$ ergs s^{-1}, which is 13% of the spin-down energy of PSR B0540−69. The fraction is again similar to that of the Crab.

N157B (PSR J0537−6910) is the only other LMC SNR with a detected pulsar (16 ms) and also shows both an extended (resolved by *ROSAT* HRI), nonthermal nebula and a partial X-ray–emitting shell (Wang & Gotthelf 1998a, 1998b). The upcoming *Chandra* observations will make a detailed comparison between these two young Crab-like SNRs possible.

We gratefully acknowledge the *Chandra* team for making available the public data used herein. In particular, we thank A. Rots and S. Murray for kindly making available their beta software. We thank U. Hwang for pointing out an instrumental artifact ("ghost image") in the original HRC image of SNR B0540−69. We thank Dick Manchester for sending us the radio image and Fernando Camilo, David Helfand, and Jules Halpern for carefully reading the manuscript. This work was funded in part by NASA LTSA grants NAG5-7935 (E. V. G.) and NAG5-6413 (Q. D. W.). This is contribution number 690 of the Columbia Astrophysics Laboratory.

REFERENCES

Chanan, G. A., Helfand, D. J., & Reynolds, S. P. 1984, ApJ, 287, L23
Clark, D. H., Tuohy, I. R., Dopita, M. A., Mathewson, D. S., Long, K. S., Szymkowiak, A. E., & Culhane, J. L. 1982, ApJ, 255, 440
Deeter, J. E., Nagase, F., & Boynton, P. E. 1999, ApJ, 512, 300
Finley, J. P., Oegelman, H., Hasinger, G., & Trümper, J. 1993, ApJ, 410, 323
Jones, T. W., et al. 1998, PASP, 110, 125
Leahy, D. A. 1987, A&A, 180, 275
Manchester, R. N., Staveley-Smith, L., & Kesteven, M. J. 1993, ApJ, 411, 756
Murray, S. S., et al. 1997, Proc. SPIE, 3114, 11
Seward, F. D., & Harnden, F. R., Jr. 1994, ApJ, 421, 581
Seward, F., D., Harnden, F. R., Jr., & Helfand, D. J. 1984, ApJ, 287, L19
Wang, Q. D., & Gotthelf, E. V. 1998a, ApJ, 494, 623
———. 1998b, ApJ, 509, L109
Weiler, K. W., & Sramek, R. A. 1988, ARA&A, 26, 295
Weisskopf, M. C., O'Dell, S. L., & van Speybroeck, L. P. 1996, Proc. SPIE, 2805, 2